A realistic molecular dynamics simulation of the plastic crystalline phase of neopentane. I. The model and its static properties

W. Breymann and R. M. Pick

Citation: The Journal of Chemical Physics **91**, 3119 (1989); doi: 10.1063/1.456934
View online: http://dx.doi.org/10.1063/1.456934
View Table of Contents: http://scitation.aip.org/content/aip/journal/jcp/91/5?ver=pdfcov
Published by the AIP Publishing

A realistic molecular dynamics simulation of the plastic crystalline phase of neopentane. I. The model and its static properties

W. Breymann[a] and R. M. Pick
Département de Recherches Physiques (U.A. 71), Université Pierre et Marie Curie, Tour 22—4, pl. Jussieu, F-75252 Paris Cedex 05, France

(Received 17 January 1989; accepted 22 May 1989)

A molecular dynamics simulation of a realistic model of neopentane [$C(CH_3)_4$] in its plastic phase has been performed on a sample of $6\times6\times6$ fcc unit cells (i.e., 864 molecules) at 135, 175, and 230 K. The molecules of the simulated sample interact through phenomenological exp-6, atom–atom potentials between all the atoms of nearest neighbor molecules. The orientational probability density function (opdf), the displacement probability density function (dpdf), and its second moment the Debye–Waller factor have been computed. We confirm the very large value and the important thermal variation of the Debye–Waller factor and the strong anisotropy of the opdf deduced from neutron diffraction experiments. The computed opdf is very well reproduced by a mean-field calculation making use only of the microscopic intermolecular potential and of the equilibrium position of the molecular centers of mass, a result in line with the isotropic character of the dpdf, but not valid for other plastic crystals made of molecules with different geometries.

I. INTRODUCTION

This article is the first of a series of papers which are devoted to a realistic molecular dynamics simulation of the rotator phase of neopentane [$C(CH_3)_4$]. Rotator phases, also named plastic or ODIC (Orientation Disorder In Crystal) phases, are thermodynamically stable phases between the solid state and the liquid state, in which the centers-of-mass of the molecules are still ordered while their orientations are disordered. An ODIC phase is thus a partially ordered state of matter which presents the advantage of offering at the same time most of the features of the disordered systems and, due to the long-range order or the center-of-mass positions, the possibility of using solid state physics techniques for the analysis of its properties; for instance, the local order in ODIC phase is very similar to what exists in a liquid, but the long-range order allows us to use the crystal space group properties to analyze the data. Studying ODIC phases can thus help understanding liquids, but is easier to do.

Up to now, different theories of rotator phases have been developed.[1] Each of them may be rather successful in the description of some of the properties, but fail on others, and a synthetic description of all the aspects of ODIC phases is actually not in view. Also, experiments on these phases are much more difficult to interpret than in ordered crystals for two reasons. Firstly, due to the orientational disorder, most data consist of smooth, often featureless functions which represents an important loss of information with respect to a fully ordered system. Secondly, the interpretation of these data depends considerably on the choice of theoretical models the validity of which are not always sure.

In such a situation, molecular dynamics (MD) simulations are extremely useful for at least three reasons:

(i) They can provide us with microscopic information (such as the position and orientation of a given molecule or set of molecules), which cannot be obtained in any real experiment.

(ii) The interaction potential between the molecules is perfectly known.

(iii) This potential can be modified at one's will, at least between certain limits.

One can thus, either test an experimental interpretation if the interaction potential is known with enough accuracy, or the validity of a theory by comparing its predictions with the actual MD results.

The shortcomings of MD simulations are nevertheless important. The size of the simulated sample is always very small and the simulated time interval extremely short compared to the size of a real crystal and to the duration of a real experiment. These facts limit very soon the frequency resolution and the number of accessible points in the Brillouin zone. MD simulation is thus a powerful tool which provides information which is, to some extent, complementary to that obtained from experiments.

During the past few years, due to the availability of large size computers, a relatively large number[2–5] of MD computations have been performed. Most of them have been devoted to comparisons with experimental results. The discrepancies have been usually attributed to the inaccuracy of the intermolecular potentials. This is the case, e.g., for CBr_4, where many of the differences between the computed results[5] and the experiments can clearly be attributed to the unrealistic form of the Br–Br interaction potential.[6] On the contrary, much less efforts have been done for the comparison between such computations and the theoretical aspects. Using a somewhat realistic potential, Lynden-Bell *et al.*[7]

[a] Permanent address: Institut für Physik, Universität Basel, Klingelbergstraße 82, CH-4056 Basel, Switzerland.

 0021-9606/89/173119-14$02.10

were the first to start such a comparison with some aspects of Michel[8,9] and also Mahanty[1,10] ideas. At the same time, a schematic 2D, and thus unrealistic model of an alkali cyanide was studied in detail by Yvinec[11,12] and Buchet and Pick[13] and revealed that the dynamical response functions obtained by MD were largely in agreement with the linear approximations of the microscopic theories in the high temperature region, but that this agreement decreases with decreasing temperature, a result yet not fully understood.

More recently, it has been noticed that the best interatomic potentials presently known (or properly approximated) are those of hydrocarbon systems with completely saturated bonds; some molecules of that type such as methane, adamantane ($C_{10}H_{16}$), bicyclo-octane [$HC(CH_2-CH_2)_3CH$], or neopentane display plastic phases. Furthermore, their interatomic potentials (C–C, C–H, or H–H interactions) can be conveniently represented[14] under analytic forms depending only on the relative distances of the two atoms. Such systems are thus the best suited for MD computations, and such computations have been recently performed on adamantane[15,16] and bicyclo-octane,[17] leading to useful microscopic information. For instance, in adamantane, the orientational probability distribution function (opdf) of the molecules, their residence time inside an orientational potential well and the major reorientation processes have been deduced from the computations and successfully compared to existing experimental data.

Having in mind to compare our results both with those of various experiments performed in our laboratory[18,19] as well as with some aspects of the microscopic theory,[9] we have decided to perform a MD simulation of neopentane and a careful analysis of the static and dynamical results which can be obtained from this simulation. The present paper is devoted to the description of the system we have studied, to the presentation of its static properties [opdf, displacement probability density function (dpdf) and its second moment, the Debye-Waller factor] as well as to their theoretical analysis. In particular, the possibility of predicting the opdf from the crystal structure and the microscopic potential alone is of primary importance, because the choice of the orientational variables which have to be used to study the various dynamical properties of the model depends on the orientations which maximize the opdf.[20] We have shortly mentioned in Ref. 21 and we shall show in detail here that, contrary to the case of at least some ionic–molecular plastic phases (see Sec. VI), a kind of mean-field description of this opdf is possible in neopentane. The dynamical properties of our model as well as an extended comparison with the translation–rotational coupling theories will be presented in forthcoming papers.[20]

The outline of this paper is as follows: In Sec. II, we give the description of the model, while Sec. III is devoted to the description of the results concerning its static properties. In the first part of Sec. III, we shall present in detail our results on the opdf, which have been shortly outlined in Ref. 22, with some remarks concerning the difficulties of representing graphically this function in the case of a three-dimensional rotator; the second part will be devoted to the description of the dpdf, together with the Debye–Waller factor thermal evolution which was found to be very large. In Sec. IV, these results will be briefly compared with the experimental ones. Section V will be devoted to the computation of the orientational mean potential, and Sec. VI, finally, to the discussion of our results.

II. DESCRIPTION OF THE MODEL

First, let us recall some experimental results about neopentane. Neopentane is a molecule with tetrahedral symmetry, where the central C atom is placed at the center of a regular tetrahedron and the C atoms of the methyl groups are placed at its corners (Fig. 1). The different bond lengths and bond angles have been determined in the liquid[24] and the vapour[25] phases, and are very similar; the precise values used in the present calculation are given in Table I. In fact, the latter are also, within the error bars, identical to those obtained in the plastic phase,[18] namely 1.58 and 2.17 Å for the distances between the central C atom and the C and H atoms of the methyl group, respectively.

Neopentane displays an ODIC phase between 140 and 256.5 K, with an entropy change of 16.4 JK^{-1} mol^{-1} at the ordered solid–plastic phase transition, which suggests that disorder must play an important role in the plastic phase. Indeed, if one neglects any contribution to the entropy change at the phase transition other than the orientational disorder (assumed to be complete above the transition), one gets the usual formula $\Delta S = R \times \log N$, where N is the number of equilibrium orientations; this yields $N = 7.2$, a value astonishingly close to the experimental value of six equivalent equilibrium orientations, in spite of the crudeness of the former approximation.

In the plastic phase, the crystal symmetry is fcc with an O_h^5 space group and a lattice parameter which varies from 8.56 ± 0.01 Å at 150 K to 8.80 ± 0.01 Å at 253 K.

In order to make the model as realistic as possible, we represented the neopentane molecule as a rigid body where all of its 17 atoms[26] are supposed, to start with, to have the

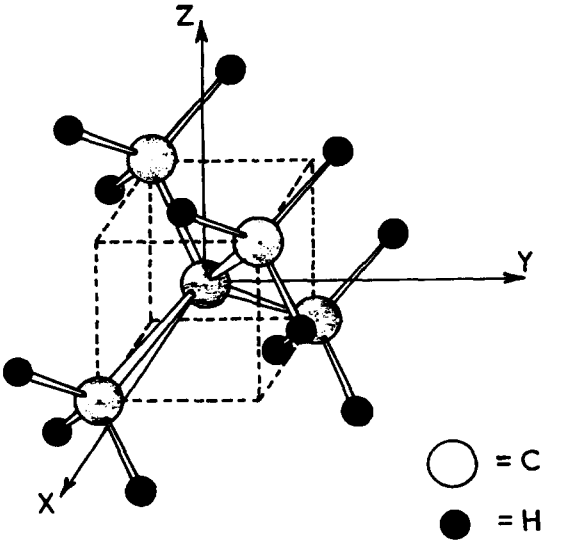

FIG. 1. Graphical representation of a neopentane molecule.

TABLE I. Numerical data pertinent to the neopentane molecule.

l(C–C)	1.62 Å
l(C_{ctr}–H)	2.228 Å
∠(C–C_{ctr}–C)	109.5°
∠(C_{ctr}–C–H)	112°
∠(H–C–H)	107°
molecular mass	$72u = 1.196\times10^{-25}$ kg
moment of inertia	2.054×10^{45} kg×m^2

experimentally measured bond length and angles. The molecules are interacting through exp-6, atom–atom potentials between all their atoms. Because of the short range of this interaction, we have limited it to nearest neighbor molecules only. No other interactions are taken into account. Thus, the potential energy of the model is given by

$$V(\Omega_i,\Omega_j,\mathbf{r}_{ij}) = \sum_{a=1}^{17}\sum_{b=1}^{17}\left[B_{ab}\exp\{-C_{ab}\cdot|\mathbf{r}_{ij}+\boldsymbol{\rho}_a(\Omega_i)-\boldsymbol{\rho}_b(\Omega_j)|\}-\frac{A_{ab}}{|\mathbf{r}_{ij}+\boldsymbol{\rho}_a(\Omega_i)-\boldsymbol{\rho}_b(\Omega_j)|^6}\right], \tag{2.1}$$

where $\mathbf{r}_{ij}=\mathbf{r}_i-\mathbf{r}_j$, $\mathbf{r}_i$ ($\mathbf{r}_j$) is the center-of-mass position of the molecule i (j), Ω_i represents the molecular orientation, and $\boldsymbol{\rho}_a(\Omega_i)$ is the relative position of atom a of molecule i with orientation Ω_i with respect to the center-of-mass position.

The values of the interaction constant A_{ab}, B_{ab}, and C_{ab} are given in Table II. They have been taken from Ref. 14.

The Hamiltonian of the system can be written as

$$H=\sum_{\langle i,j\rangle}V(\Omega_i,\Omega_j,\mathbf{r}_{ij})+\frac{1}{2m}\sum_i p_i^2+\frac{1}{2\theta}\sum_i L_i^2, \tag{2.2}$$

where m is the molecular mass, θ the molecular moment of inertia, and $\langle\ \rangle$ represents a summation over all nearest neighbor pairs.

One of our aims was to study time and space correlation functions of the simulated system. In order to have access to a sufficiently large number of points in the reciprocal lattice, the sample must not be too small. We choose it to be formed of 6×6×6 fcc unit cells (corresponding to a system with 864 molecules) repeated periodically in space. The test runs lead to reasonable results for the various macroscopic quantities, so that we only decreased the H–C–H bond angle by approximately 2.5° (which lies within the accuracy of the experimental results) in order to produce a slightly less isotropic potential. This change of potential might explain why the lattice parameter, at reasonable pressure (cf. Table III) is approximately 2% larger than the experimental value. Nevertheless, as will be seen below, the opdf produced by the simulation is still too isotropic, compared with the experimental results. The reason for this discrepancy will be discussed in some more detail in Sec. IV and makes us propose that the too large lattice parameter is, mostly, an indirect effect of the too isotropic opdf.

TABLE II. Coefficients of the atomic interaction $V_{ab} = -A_{ab}r^{-6} + B_{ab}\cdot\exp(-C_{ab}r_{ab})$.

Interacting atoms	$A\left[\frac{\text{kcal}\times\text{Å}^{-6}}{\text{mol}}\right]$	$B\left[\frac{\text{kcal}}{\text{mol}}\right]$	$C[\text{Å}^{-1}]$
C–C	568	83 630	3.6
C–H	125	8 766	3.67
H–H	27.3	2 654	3.74

TABLE III. Specifications of the runs. Note that, due to the constraints of the box, at 135 K, the model is still in the ODIC phase.

Run n°	1	2	3
Number of particles		864	
Symmetry		fcc	
Time step		10 fs	
Duration (time steps)		6000	
Cell parameter (Å)	8.768	8.854	9.03
Temperature (K)	137 ± 2	173 ± 2	232 ± 3
Total energy (kJ/mol)	−20.93	−18.66	−14.89
Potential energy (kJ/mol)	-24.35 ± 0.05	-22.97 ± 0.05	-20.68 ± 0.07
Virial (kJ/mol)	0.2 ± 1.2	-1.5 ± 1.5	0.7 ± 1.7
Pressure (MPa)	11 ± 4	18 ± 4	15 ± 5

With the 864 molecule sample, we have performed three different constant volume[28] runs at 135, 175, and 230 K, which cover nearly the whole temperature range of the ODIC phase of neopentane. The duration of the runs was 8000 time steps of 10^{-14} s., the first 2000 steps being used for the thermalization process. During the run, the total energy, the potential energy, the virial, the pressure, and the temperature of the sample were monitored. Their mean values are shown in Table III. The total energy does not shift during the run, its fluctuations are of the order of one percent of the fluctuations of the kinetic energy.

III. STATIC PROPERTIES

This section is divided into two subsections. In the first one, the results concerning the opdf will be presented; in the second one, we shall describe those concerning the Debye–Waller factor and the dpdf.

A. The orientational probability density function

The opdf of a crystal with N molecules, which was simulated during M time steps, is given through

$$\mathscr{P}(\Omega)=\frac{1}{8\pi^2NM}\sum_{i=1}^{N}\sum_{j=1}^{M}\delta[\Omega-\Omega_i(t_j)], \tag{3.1}$$

where $\Omega_i(t_j)$ represents the orientation of the molecule i at time step j. This function is difficult to represent graphically, since it depends on three variables (e.g., the three Euler angles). For this purpose, it is better to look at the odpf of the C–C molecular bonds. This quantity depends on two spherical angles only

$$p(\hat{\mathbf{r}})=\frac{1}{4NM}\sum_{i=1}^{N}\sum_{j=1}^{M}\sum_{k=1}^{4}\delta\{\hat{\mathbf{r}}-\hat{\mathbf{r}}_k[\Omega_i(t_j)]\}, \tag{3.2}$$

where $\hat{\mathbf{r}}$ is a unity vector which represents the spherical angles and $\hat{\mathbf{r}}_k$ is the direction of the C_{ctr}–C_k bond, C_{ctr} being

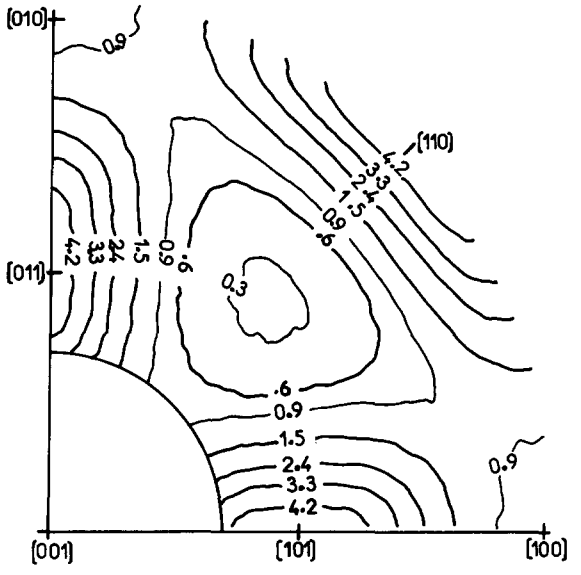

FIG. 2. Histogram of the C–C bond opdf at 135 K.

the central atom and C_k one of the four outer carbon atoms of a neopentane molecule. In general, there is no strict one-to-one correspondence between both functions, but the second gives a general overview of the orientational probability.

Figure 2 shows a stereographic projection of $p(\hat{\mathbf{r}})$ for the lowest temperature simulation. The function presents pronounced maxima in the [110] directions, absolute minima in the [111] directions, and secondary minima in the [100] directions. Between the [111] and [100] minima, it has saddle points. These features are characteristic for a molecular

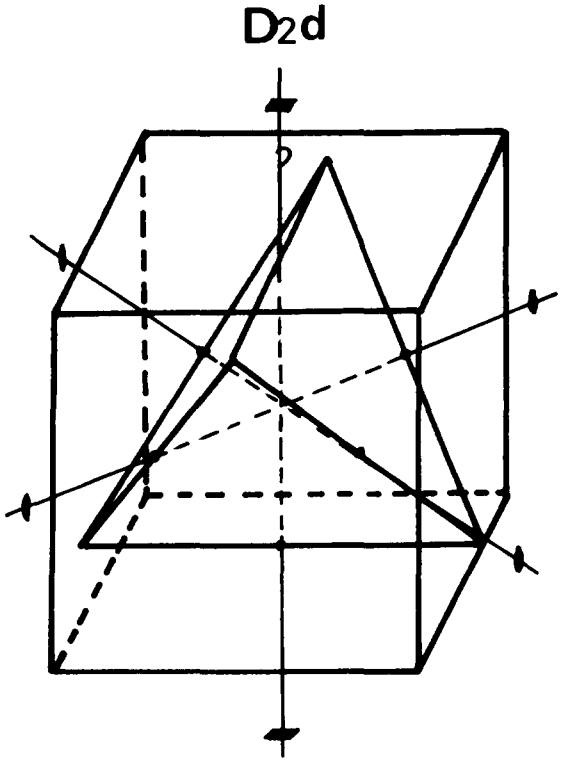

FIG. 3. A tetrahedron in D_{2d} orientation.

orientation with D_{2d} symmetry, for which one $\bar{4}$ molecular axis coincides with a fourfold crystal axis (e.g., the z axis), while the two other $\bar{4}$ molecular axes point in [110] directions of the crystal perpendicular to that crystal fourfold axis (Fig. 3), which gives rise to six equivalent, but physically distinct such orientations. The [110] direction of the maxima of $p(\hat{\mathbf{r}})$ as well as their elongation toward the [100] directions are easily explained by the fact that the C–C bonds of a molecule in a D_{2d} orientation point nearly in a [110] direction, but with a slight displacement toward a [100] direction.

From a mathematical standpoint, the opdf $\mathscr{P}(\Omega)$ can be developed on a basis of symmetric rotator functions $\mathscr{R}_l^{\lambda\lambda'}(\Omega)$. These functions, first introduced by Hüller and Press[29] and more systematically studied by Yvinec and Pick[30,31], are appropriate linear combinations of Wigner rotator functions $D_l^{mm'}(\Omega)$ with the same l. They have the important property of being adapted simultaneously to both the crystal and molecular symmetries. The development of $\mathscr{P}(\Omega)$ in a series of those functions reads

$$\mathscr{P}(\Omega)=\sum_{l\lambda\lambda'}\frac{2l+1}{8\pi^2}A_l^{\lambda\lambda'}R_l^{\lambda\lambda'}(\Omega). \tag{3.3}$$

Here, $\lambda=(\Gamma,\mu,n)$ and $\lambda'=(\Gamma',\mu',n')$ are composite indices, where Γ (Γ') represents an irreducible representation with respect to the site (molecular) symmetry point group, μ (μ') labels the different representations Γ (Γ'), if Γ (Γ') is contained more than once in a given l subspace, and n (n') numbers the one-dimensional subspaces of Γ (Γ'). The coefficients $A_l^{\lambda\lambda'}$ can be computed easily using Eqs. (3.1) and (3.3) and the orthogonality relation of the symmetric rotator functions.

Due to the high molecular and crystal symmetries, only some coefficients are nonzero, as it can be shown that[30]:

(i) either λ and λ' belong, respectively, to the unity representation of the site and the molecular point group symmetries; the corresponding coefficients are called coefficients of the first kind;

(ii) both, λ and λ', belong to the one-dimensional representation of their group which has a character equal to 1 for all the proper rotations and to -1 for all the improper rotations. The corresponding representations are the A_2 and the A_{1u} representation for T_d and O_h point symmetry groups, respectively.

In order to simplify the notation, these terms will be labeled with indices (1) and (2), respectively, so that Eq. (3.3) simplifies to

$$\mathscr{P}(\Omega)=\sum_l\frac{2l+1}{8\pi^2}[A_l^{(1)}\mathscr{R}_l^{(1)}(\Omega)+A_l^{(2)}\mathscr{R}_l^{(2)}(\Omega)], \tag{3.4}$$

where we have made use of the fact that for the case under study and the values of l used here, there is at most one $A_l^{(p)}$ for each l. Indeed, for a T_d molecule in an O_h crystal lattice and for $l\leqslant 10$, there arises only one nonzero coefficient of the first kind for $l=4$, 6, 8, and 10 (while A_0 is fixed to 1 by normalization) and one coefficient of the second kind for $l=9$.[30]

For the computation of the coefficients $A_l^{\lambda\lambda'}$, all sym-

TABLE IV. Symmetric rotators $\mathscr{R}_l^{(1)} \equiv \mathscr{R}_l^{A_1 g A_1}$ written as functions of the C–C bond directions. $[\mathscr{S}_l]$ represents the term under the Σ sign for the corresponding l. For the expression of cubic harmonics, see, e.g., Ref. 33 and 34.

$$\mathscr{R}_0 = 1$$

$$\mathscr{R}_4^{A_1 g A_1} = -\frac{15}{16}\sum_{i=1}^{4}\left(x_i^4 + y_i^4 + z_i^4 - \frac{3}{5}\right)$$

$$\mathscr{R}_6^{A_1 g A_1} = \frac{2079}{128}\sum_{i=1}^{4}\left(x_i^2 y_i^2 z_i^2 + \frac{1}{22}[\mathscr{S}_4] - \frac{1}{105}\right)$$

$$\mathscr{R}_8^{A_1 g A_1} = \frac{1755}{64}\sum_{i=1}^{4}\left(x_i^8 + y_i^8 + z_i^8 - \frac{28}{5}[\mathscr{S}_6] - \frac{210}{143}[\mathscr{S}_4] - \frac{1}{3}\right)$$

$$\mathscr{R}_{10}^{A_1 g A_1} = \frac{26\,163}{5504}\sum_{i=1}^{4}\left(x_i^{10} + y_i^{10} + z_i^{10} - \frac{45}{19}[\mathscr{S}_8] - \frac{126}{17}[\mathscr{S}_6] - \frac{210}{143}[\mathscr{S}_4] - \frac{3}{11}\right)$$

metric rotator functions can be expressed directly in terms of quaternions, as has been done for the functions $\mathscr{R}_3^{A_1 u A_2}(\Omega)$, $\mathscr{R}_4^{A_1 g A_1}(\Omega)$, and $\mathscr{R}_6^{A_1 g A_1}(\Omega)$ in Ref. 32. Here, however, we will use another approach, valid for functions with $l < 12$ being in the unity representation of the molecular symmetry group. This technique allows us to compute the coefficients of the series development (3.4) with the help of functions depending on two spherical angles only (Table IV); indeed, using Eq. (A7) of Appendix A, one can write for the coefficients of the first kind

$$A_l^{(1)} = \frac{1}{4NM\mathscr{M}_l^{A_1}(\hat{\mathbf{r}}_0)}\sum_{i=1}^{N}\sum_{j=1}^{M}\sum_{k=1}^{4}\mathscr{S}_l^{A_1 g}\{\hat{\mathbf{r}}_k[\Omega_i(t_j)]\}, \tag{3.5}$$

where the different functions $\mathscr{S}_l^{\lambda}$ ($\mathscr{M}_l^{\lambda}$) are site (molecular) symmetry adapted spherical harmonics, $\hat{\mathbf{r}}_0$ represents the direction of an arbitrary C_0–C_k bond described in the molecular axes, and $\hat{\mathbf{r}}_k[\Omega_i(t_j)]$ the same quantity for molecule i at instant t_j, described in the crystal axes. Using Eq. (A9) of the same appendix, the formula for the coefficient of the second kind $A_9^{(2)}$ can be derived in the same manner.

The first four coefficients $A_l^{(1)}$ for our three runs have been computed in this manner. They are displayed as a function of temperature in Fig. 4(a). The essential feature for the D_{2d} orientation is a small A_4 and a highly negative A_6 coefficient (cf. Table V), which is the case in Fig. 4(a). Furthermore, there is a weak, but definite variation of these coefficients with temperature, this variation being linear within the limits of the error bars.

Limiting the expansion in Eq. (3.4) to $l \leqslant 10$, a complete description of $\mathscr{P}(\Omega)$ cannot, of course, be obtained. In order to illustrate the effects of such a series truncation on the opdf, we finally present in Fig. 5 a stereographic projection of a limited development of the C–C bond opdf $p(\hat{\mathbf{r}})$ for the lowest temperature simulation, which only contains terms with $l \leqslant 10$.[35] Compared with Fig. 2, one clearly notices the larger width of the maxima towards the [111] directions. This difference between both figures is a visible effect of the limited expansion of the opdf. It is due to the fact that the series truncation limits the steepness of the flanks of the rep-

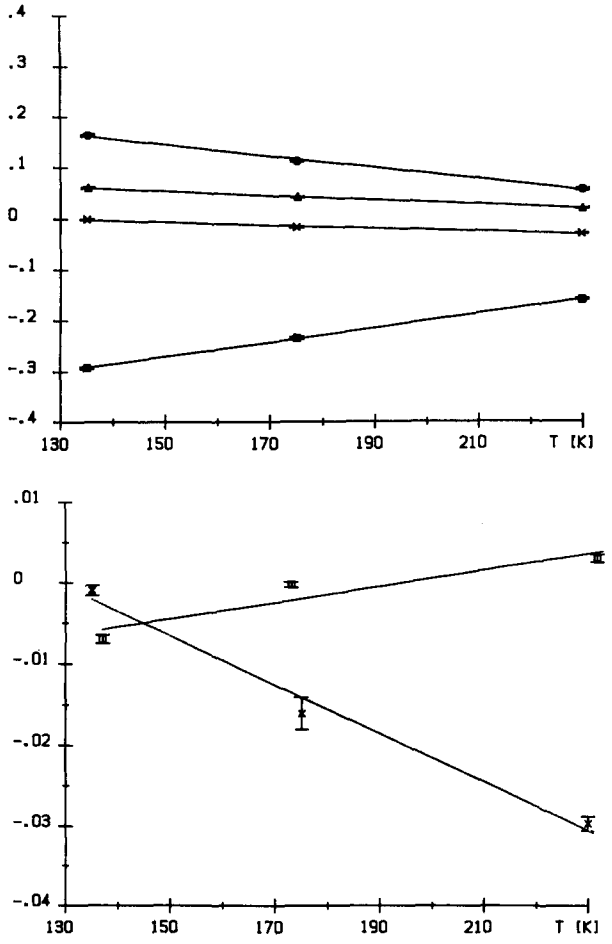

FIG. 4. Variation of the coefficients of the opdf with temperature. (a) Coefficients of the first kind: $A_4(\times)$, $A_6(\square)$, $A_8(\bigcirc)$, and $A_{10}(\triangle)$. (b) The first coefficient of the second kind, $A_g^{(2)}$ (III), compared with $A_4^{(1)}(\times)$. Note the differences in scale.

TABLE V. Coefficients $A_l^{(1)}$ for an ideal D_{2d} orientation.

l	$A_l^{(1)}$
0	1
4	0.166 666 7
6	−0.75
8	0.708 335
10	0.312 512

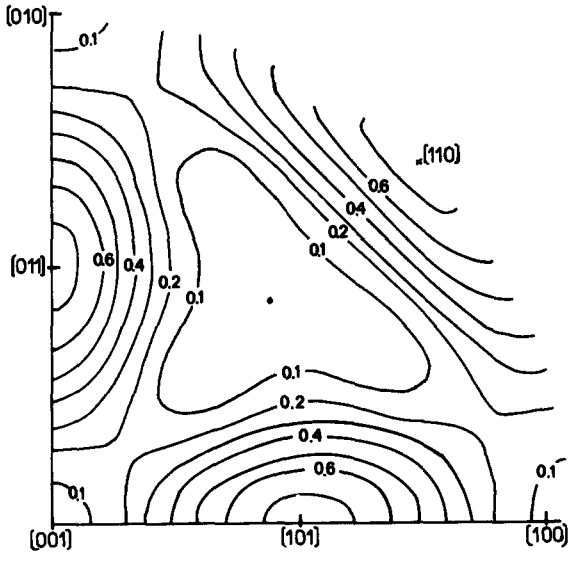

FIG. 5. Histogram of the limited development of the C–C bond opdf at $T = 135$ K. (Scale not the same as in Fig. 2).

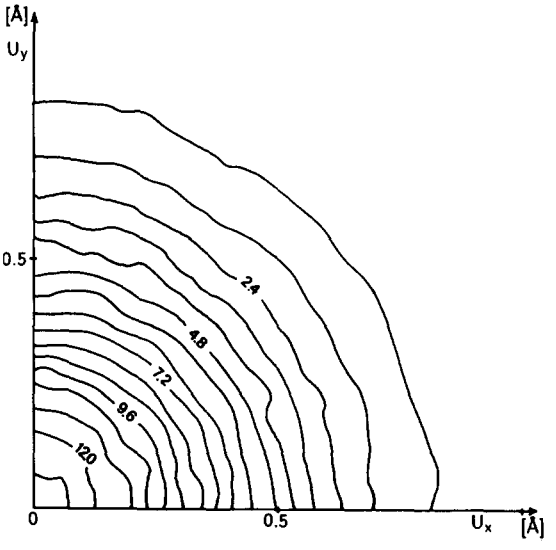

FIG. 6. Histogram of the dpdf [cut through the (001) plane at $u_z = 0$].

resented function.[36] As the opdf is more isotropic at higher temperature, one expects that the difference between the histogram and the limited development would diminish. Indeed, there is practically no difference between the two stereographic projections at 230 K.

Figure 4(b) represents the thermal evolution of $A_4^{(1)}$ and that of $A_9^{(2)}$ on an expanded scale. This last figure, reproduced from Ref. 22, describes the first determination of a coefficient of the second kind. We have argued in Ref. 22 that its small numerical value was definitely not zero, at least for two of the three temperatures used in the present calculation.

The fact that no $A_9^{(2)}$ coefficient had ever been measured before needs to be substantiated, because Meyer and Ciccoto[15] have suggested that they have obtained this coefficient in adamantane by a MD technique similar to ours, and they found it to be zero within the limit of accuracy of their computation. In fact, these authors did not develop the opdf through Eq. (3.4), but rather $p(\hat{\mathbf{r}})$ with the help of the equation of Ref. 35; they computed the corresponding expansion coefficients a_l^λ with a technique similar to Eq. (3.5), namely

$$a_l^\lambda = \frac{1}{4NM} \sum_{i=1}^{N} \sum_{j=1}^{M} \sum_{k=1}^{4} \mathcal{S}_l^\lambda \{\hat{\mathbf{r}}_k [\Omega_i(t_j)]\}. \tag{3.6}$$

Using Eqs. (A6) of Appendix A, one finds that by applying this technique, one obtains quantities which are proportional to the coefficients $A_l^{\lambda A_1}$ of Eq. (3.3), i.e., to coefficients of the first kind which should imply $\lambda = A_{1g}$. Unfortunately, as shown in Ref. 30, there is only a coefficient of the second kind for $l = 9$, which means that $A_9^{\lambda A_1} = 0$ whatever is the one-dimensional representation λ. In Ref. 15, λ has been chosen as $\lambda = A_{1u}$, and in agreement with the previous discussion, it has been found that $a_9^{A_{1u}}$ was equal to zero, within the accuracy of the calculation, but no information on $A_9^{(2)}$ can be deduced from such a result.

B. Displacement probability density function and DW factor

Using the same technique as in Eq. (3.1), we have computed the center of mass displacement probability density function (dpdf), which is defined as

$$d(\mathbf{u}) = \frac{1}{NM} \sum_{i=1}^{N} \sum_{j=1}^{M} \delta[\mathbf{u} - \mathbf{u}_i(t_j)], \tag{3.7}$$

where $\mathbf{u}_i$ is the center-of-mass displacement of the ith molecule. Contrary to the opdf, this function is quite isotropic as is shown in Fig. 6, which represents a histogram of this function in the (001) plane, and we have verified that the same result holds for sections of this function by other plans. Furthermore, a cut of the function through a [100] axis shows that it has a quite perfect Gaussian shape (Fig. 7).

$d(\mathbf{u})$ is not a function easily attainable through a diffraction experiment. In order to allow for an easier comparison with experiment, one needs to compute the Debye–Waller factor

$$\langle u_x^2 \rangle = \frac{1}{NM} \sum_{i=1}^{N} \sum_{j=1}^{M} u_{ix}^2(t_j), \tag{3.8}$$

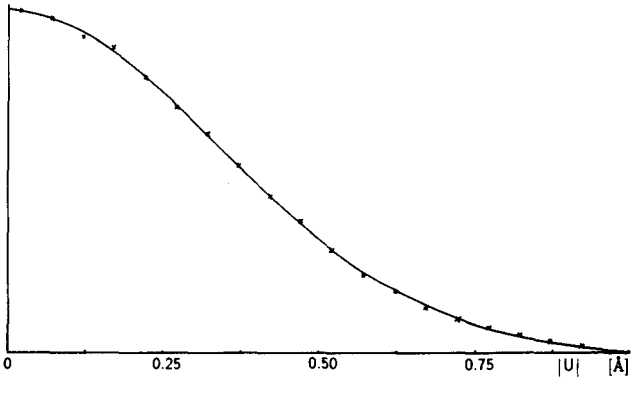

FIG. 7. Radial dependence of the dpdf ($\times$) fitted with a Gaussian curve.

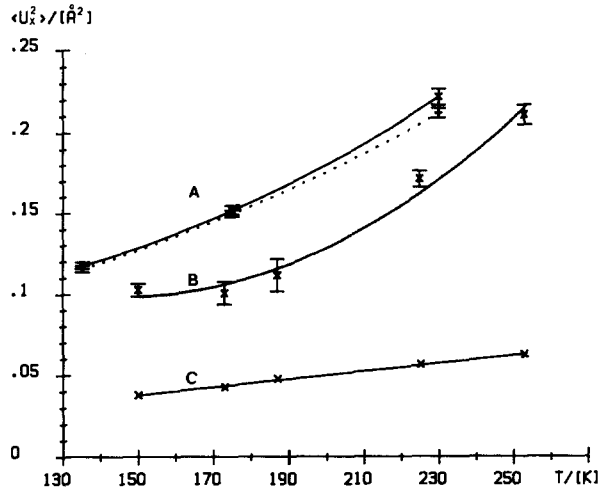

FIG. 8. Temperature dependence of the Debye–Waller factor. (a) MD calculation. (b) Experimental values (Ref. 18). (c) Theoretical values calculated with a Debye model (Ref. 18).

where $u_{ix}(t_j)$ is the center-of-mass displacement of the ith molecule in the x direction at instant t_j. It is plotted as a function of temperature on Fig. 8. On the same figure, we have represented the experimental values obtained in the neutron elastic scattering experiment of Denise *et al.*[18] and a theoretical curve which was computed in the same reference for a Debye isotropic model. The conclusion which can be drawn from these curves will be summarized in the next section.

IV. COMPARISON WITH EXPERIMENTS

A. General remarks

Ideally, one would like to extract from the experiment precise information such as the opdf and/or the Debye–Waller factor and compare it with the results of an MD simulation. This is, in practice, impossible because this information is always obtained through the use of a (more or less) simplified model of the ODIC phase in which various approximations are performed, the validity of which are not always obvious. Consequently, the experimental results [e.g., the shape of the opdf, or more precisely, the values of the coefficients appearing in Eq. (3.4)] may be affected not only by the experimental uncertainties, but also by the inaccuracy or the crudeness of the model used for the data analysis.

Our present knowledge of the static properties of neopentane has been deduced from elastic neutron scattering experiments performed by Denise *et al.*[18,19] In order to avoid the above-mentioned difficulties, a comparison between our MD simulation and these data has been made[23] using the following procedure: We have first computed Bragg peak intensities with the help of our MD data. Then, these computed intensities have been analyzed with the theoretical model which had been used in the experimental data analysis and was designed to yield the first four nontrivial first kind coefficients of Eq. (3.4) and the value of the Debye–Waller factor. Would the model be totally appropriate, the values for the coefficients of Eq. (3.4) and for the Debye–Waller factor extracted through the *computed* Bragg peaks should be the same as those obtained in Sec. III. Conversely, any discrepancy between the two sets of data will be related to defects of the model used for the data analysis and will therefore cause some doubts on further comparisons between the MD results and the information extracted from the experiment.

B. Discussion of the opdf and of the DW factor: Validity of the potential

Using the technique just described, we have found that the opdf deduced from the two ways of treating the MD data had similar characteristics: both have maxima for the D_{2d} orientations and minima of $p(\hat{\mathbf{r}})$ for the [111] directions. Furthermore, the general decrease of the coefficients $A_6^{(1)}$, $A_8^{(1)}$, and $A_{10}^{(1)}$ with increasing temperature, apparent on Fig. 4(a), is obtained through both methods of treating the data. Nevertheless, the uncertainties in the numerical values obtained through the auxiliary computation of the Bragg peaks is much larger than those reported on Fig. 4(a). This fact indicates that the model used for extracting these coefficients from the Bragg peaks is rather crude, and that the comparison between the experimental and the simulated opdf obtained with the help of such a model can only be semiquantitative. Within such limits, the MD simulation and the neutron scattering experiment cannot really be differentiated.

Interestingly enough, the two Debye–Waller factors extracted from the two treatments of the MD data (full and dotted lines of curve A in Fig. 8) are identical and obtained with a similar accuracy. The discrepancy between curves A and B of Fig. 8 is thus real and indicates the existence of inaccuracies of the interaction potential described in Sec. II. Nevertheless, both curves are practically proportional to one another over the whole temperature range and do not differ by more than approximately 25%. The interaction potential used in the present calculation is thus good enough to describe the important features of the neopentane ODIC phase in the whole temperature range. Its failure to give an exact description of all its properties is not surprising. Indeed, such potentials have been used for comparisons with experimental data related to crystal lattice parameters[37] as well as harmonic and anharmonic dynamics.[38] They give good agreement for quantities such as phonon frequencies and linewidths between the computed and the experimental values. Nevertheless, during reorientation processes, the hydrogen atoms of neighboring molecules approach each other much more than in an ordered crystal. They reach a distance for which the phenomenological exp-6 potential is no longer valid and, presumably, not steep enough. This observation is in line with recent results of Righini *et al.*[39] who found that in the case of methane, at short distances, this potential is too soft compared to the real potential. This too soft character of the exp-6 potential will have some important consequences in the comparison of the dynamical MD results with the experimental one. The experimental lifetime of a molecule in its potential well will be longer than the computed one. Indeed, in such a case, its detection would be only limited by its too large bandwidth; as discussed in Ref. 12, the latter con-

tains a static contribution, related to the influence of the orientational disorder on the force constants, and a dynamical contribution due to the residence time of a molecule in an orientational potential well. The inaccuracy of our potential decreases the residence time and thus adds an artificial bandwidth which does not exist in the actual crystal. Within such limitations, comparison between an MD simulation and experimental data will be possible, as expected in the introduction.

C. Further comparison with experiment: Coefficient of the second kind; $d(\mathbf{u})$ and the Debye–Waller factor

As pointed out in Sec. IV A, the similarity between the simulated system and real neopentane does not mean that information obtained from the simulation can always be compared with experiment. A first example is given by the coefficient of the second kind $A_l^{(2)}$ for $l=9$. The only experimental method proposed so far to measure it[31] is an analysis of the elastic part of an incoherent inelastic neutron scattering experiment. This part is, in itself, difficult to measure and the analysis of the data implies the use of spherical Bessel functions of the order $l=9$, which are almost zero for all the transferred wave vectors which are accessible in such an experiment. Thus, though the numerical value of $A_9^{(2)}$ is of the same order of magnitude as $A_4^{(1)}$, it is more difficult to measure; any comparison between our results and the real crystal is not presently forseeable.

A second, and different, aspect is given by the thermal behavior of the Debye–Waller factor. The comparison of curves A or B with curve C of Fig. 8 indicates that the translational phonons cannot be the sole origin of the large value of this quantity and of its thermal behavior. Reanalyzing their data with a more sophisticated model than in Ref. 18, Depondt *et al.*[19] have shown that neopentane molecules had orientations more localized in the vicinity of ideal D_{2d} ones than is apparent using a stereographic projection. Depondt and Galam[40] further suggested that the molecules would reorient only when *all* the 12 nearest neighbors are displaced by an amount such that their relative distance is twice their van der Waals radius, so that steric hindrance does no longer exist. Using an Arrhenius type reorientational probability, they showed that their model was compatible with all the experimental data and could completely explain the difference between curves B and C at all but the lowest temperature ($T=137$ K) without using any adjustable parameter. This extra contribution to the Debye–Waller factor gives a displacement pattern for each neighboring ion of the reorienting molecule in the vicinity of one of the 12 [110] directions, thus a fairly isotropic total contribution; the normal phonon contribution is also quite isotropic in a cubic crystal. One thus expects an isotropic $d(\mathbf{u})$, which is actually found (cf. Fig. 6).

Let us stress that if, conversely, the difference between curves B and C would be related to a coupling between the orientation of a molecule and the displacement of its center-of-mass in a particular direction (cf. Sec. V), a rather anisotropic $d(\mathbf{u})$ would be expected, because the opdf is quite anisotropic. The isotropy of $d(\mathbf{u})$ shown in Fig. 6 agrees with the Depondt and Galam picture[40] and is thus an indirect support to their model, even if $d(\mathbf{u})$ is not experimentally attainable.

On the other hand, there is no reason for the extra contribution to $d(\mathbf{u})$ to have a Gaussian shape distribution. As this contribution is the dominant part of $d(\mathbf{u})$, we cannot offer an explanation for this aspect of our result.

V. COMPARISON WITH THEORY

A. The orientational mean potential

In the preceding section, we have extracted from a MD simulation two monomolecular static quantities, the displacement probability density function $d(\mathbf{u})$ and its orientational counterpart the opdf $\mathscr{P}(\Omega)$. The prediction of these quantities, starting simply from the two molecule interaction potential, is an important problem for the theory of ODIC phase. In the case of $\mathscr{P}(\Omega)$, this problem can, of course, be formally transformed through the use of an effective one-particle orientational potential $\overline{V}(\Omega)$ into

$$\mathscr{P}(\Omega)=e^{-\beta\overline{V}(\Omega)}, \tag{5.1}$$

where $\overline{V}(\Omega)$ is defined as

$$\overline{V}(\Omega)=\sum_{i=1}^{12}\int d\Omega_i\int d^3r_i\,\mathscr{P}(\{\Omega_i,\mathbf{r}_i\})_{\Omega}\,V(\Omega,\Omega_i,\mathbf{r}_i). \tag{5.2}$$

In this expression, $V(\Omega,\Omega_i,\mathbf{r}_i)$ is the potential energy between the two molecules when the molecule under consideration has orientation Ω, its ith nearest neighbor being at the relative distance r_i, and having the orientation Ω_i, and $\mathscr{P}(\{\Omega_i,\mathbf{r}_i\})_{\Omega}$ is the probability of finding the nearest neighbors i with orientations Ω_i at the relative distances $\mathbf{r}_i$ when the molecule under consideration has the orientation Ω.

Since the probability $\mathscr{P}(\{\Omega_i,\mathbf{r}_i\})_{\Omega}$ in Eq. (5.2) is not known, severe approximation have to be performed for making use of this equation. The first one consists in neglecting all the correlations appearing in $\mathscr{P}(\{\Omega_i,\mathbf{r}_i\})_{\Omega}$, i.e., the correlations between the orientation of two different molecules on the one hand, and between the orientation and the displacement of the same particle on the other hand. This approximation simplifies Eq. (5.2) into

$$\overline{V}(\Omega)=\sum_{i=1}^{12}\int d\Omega_i\,\mathscr{P}(\Omega_i)\int d^3r_i\,p(\mathbf{r}_i)V(\Omega,\Omega_i,\mathbf{r}_i). \tag{5.3}$$

In Eq. (5.3), $p(\mathbf{r}_i)$ is the probability of finding two molecules at the relative position $\mathbf{r}_i$. If $\mathbf{R}_i$ represents their relative equilibrium position and $\mathbf{u}$ (respectively, $\mathbf{u}_i$) their displacement with respect to their equilibrium positions, again neglecting correlation effects, $p(\mathbf{r}_i)$ is related to the dpdf $d(\mathbf{u})$ by

$$\begin{aligned}p(\mathbf{r}_i)&=\int d^3u\int_{\mathbf{u}_i=\mathbf{r}_i+\mathbf{u}-\mathbf{R}_i} d^3u_i\,d(\mathbf{u})d(\mathbf{u}_i)\\&=\int d^3u\,d(\mathbf{u})d(\mathbf{r}_i+\mathbf{u}-\mathbf{R}_i).\end{aligned} \tag{5.4}$$

In analogy with $\mathscr{P}(\Omega)$ and within the same decoupling approximation, $d(\mathbf{u})$ can be expressed as

$$d(\mathbf{u})=e^{-\beta\overline{V}(\mathbf{u})} \tag{5.5}$$

with

$$\overline{V}(\mathbf{u}) = \sum_{i=1}^{12} \int d\Omega\, \mathscr{P}(\Omega) \int d\Omega_i\, \mathscr{P}(\Omega_i) \int d^3u_i\, d(\mathbf{u}_i) \times V(\Omega,\Omega_i,\mathbf{R}_i + \mathbf{u}_i - \mathbf{u}). \quad (5.6)$$

The five relations (5.1) and (5.3)–(5.6) represent a system of five integral equations which couple $\mathscr{P}(\Omega)$ and $d(\mathbf{u})$. It should be solved self-consistently for each temperature, which represents a very heavy and time consuming program; here we have therefore looked for approximate solutions.

Developing the two-molecule potential energy in the vicinity of the equilibrium position $\mathbf{R}_i$, one can write

$$V(\Omega,\Omega_i,\mathbf{r}_i) = V^{(0)}(\Omega,\Omega_i) + (\mathbf{u}_i - \mathbf{u})\cdot\mathbf{V}^{(1)}(\Omega,\Omega_i) + \cdots, \quad (5.7)$$

where

$$V^{(0)}(\Omega,\Omega_i) = V(\Omega,\Omega_i,\mathbf{R}_i)$$

and

$$\overline{\mathbf{V}}^{(1)}(\Omega,\Omega_i) = [\mathrm{grad}_{\mathbf{r}} V(\Omega,\Omega_i,\mathbf{r}_i)]\mathbf{r}_{i=\mathbf{R}_i}.$$

The second term of the right-hand side of Eq. (5.7) is called the linear (in displacement) translation orientation coupling energy; this and higher-order terms in displacements have been considered in the work of Michel and collaborators.[9] If the role of the translation–orientation coupling can be neglected in Eq. (5.3), as was indicated in Sec. IV C, the system of self-consistent equations for $\mathscr{P}(\Omega)$ and $d(\mathbf{u})$ may be decoupled, and Eq. (5.3) simplifies into

$$\overline{V}(\Omega) = \sum_{i=1}^{12} \int d\Omega_i\, \mathscr{P}(\Omega_i) V^{(0)}(\Omega,\Omega_i) \quad (5.8)$$

leading to a system of Eqs. (5.1) and (5.8), which may be solved in an iterative manner.

From a practical point of view, the same symmetry considerations hold for $\mathscr{P}(\Omega)$ and $\overline{V}(\Omega)$ [cf. Eq. (3.4)], so that one can write unambiguously

$$\overline{V}(\Omega) = \sum_{l} [v_l^{(1)} \mathscr{R}_l^{(1)}(\Omega) + v_l^{(2)} \mathscr{R}_l^{(2)}(\Omega)] \quad (5.9)$$

for $l \leqslant 10$. On the other hand, we can write the development of $V^{(0)}(\Omega,\Omega_i)$ as

$$V^{(0)}(\Omega,\Omega_i) = \sum_{\substack{l\lambda \\ l'\lambda'}} C_{\mathbf{R}_i}\binom{\lambda\lambda'}{ll'} \mathscr{R}_l^{\lambda A_1}(\Omega) \mathscr{R}_{l'}^{\lambda' A_1 *}(\Omega_i), \quad (5.10)$$

where we have taken into account the fact that $V^{(0)}(\Omega,\Omega_i)$ is invariant under any proper rotation of the molecular point group, and that we do not need to take into account the coefficients of the second kind, because we shall later on limit ourselves to $l \leqslant 8$ for the coefficients of the interaction potential.

Substituting Eq. (5.10) for $V^{(0)}(\Omega,\Omega_i)$ and Eq. (3.4) for $\mathscr{P}(\Omega)$ in Eq. (5.8) yields

$$\overline{V}(\Omega) = \sum_{i=1}^{12} \sum_{ll'\lambda'} C_{R_i}\begin{pmatrix} \lambda A_{1g} \\ l\ l' \end{pmatrix} A_{l'}^{(1)} \mathscr{R}_l^{\lambda A_1}(\Omega), \quad (5.11)$$

$$= \sum_{i=1}^{12} \sum_{ll'} C_{\mathbf{R}_i}\begin{pmatrix} A_{1g} A_{1g} \\ l\ l' \end{pmatrix} A_{l'}^{(1)} \mathscr{R}_l^{(1)}(\Omega), \quad (5.12)$$

where we have made use of the orthogonality relations of the rotator functions to obtain Eq. (5.11), and of the symmetry of $\overline{V}(\Omega)$ to go from Eq. (5.11) to Eq. (5.12). Comparing Eq. (5.12) to Eq. (5.9), we finally obtain for the coefficients $v_l^{(1)}$:

$$v_l^{(1)} = \sum_{l'} C_{ll'} A_{l'}^{(1)} \quad (5.13)$$

with

$$C_{ll'} = \sum_{i=1}^{12} C_{\mathbf{R}_i}\begin{pmatrix} A_{1g} A_{1g} \\ l\ l' \end{pmatrix}. \quad (5.14)$$

The coefficients $C_{ll'}$ are microscopic quantities associated with the intermolecular interaction potential and the crystal lattice symmetry. They depend only on $\mathbf{R}_i$ and can be computed from Eq. (5.10) with the help of the orthogonality relations.

Using Eqs. (5.1), (5.9), and (5.13), one can now perform a self-consistent calculation for the coefficient of $\mathscr{P}(\Omega)$ and $\overline{V}(\Omega)$, where at the ith step, one has

$$v_{l,i}^{(1)} = \sum_{l'} C_{ll'} A_{l',i-1}^{(1)}, \quad (5.15)$$

$$A_{l,i}^{(1)} = \frac{\int d\Omega_i\, \mathscr{R}_l^{(1)*}(\Omega) \exp\{-\beta \Sigma_{l'} v_{l',i}^{(1)} \mathscr{R}_{l'}^{(1)}(\Omega)\}}{\int d\Omega_i \exp\{-\beta \Sigma_{l'} v_{l',i}^{(1)} \mathscr{R}_{l'}^{(1)}(\Omega)\}}. \quad (5.16)$$

Let us point out that due to the appearance of the exponential function in Eq. (5.16), we need in principle to know at each step *all* the coefficients $v_{l,i}^{(1)}$ [as well as the contribution of the coefficients of the second kind to the exponent of Eq. (5.16), which has been systematically omitted here]. In our case, this is not important because, in a first attempt to make use of the preceding procedure, we have limited ourselves to the first step ($i = 1$) of the self-consistent calculation and to coefficients with $l \leqslant 8$ for the coefficients $v_{l,1}^{(1)}$ and with $l \leqslant 10$ for $A_{l,1}^{(1)}$. As the initial condition, we have chosen

$$A_{l,0}^{(1)} = \delta_{l,0}, \quad (5.17)$$

which represents an isotropic distribution of the neighboring molecule opdf and already gives quite interesting results, as we shall see in Sec. V C.

B. Practical computation of $\overline{V}(\Omega)$

In order to perform the numerical calculation of $\overline{V}(\Omega)$, we have fully exploited the symmetry of the two-molecule potential energy, which is invariant under a rotation of the two molecules around their common axis. Since the symmetrized rotator functions in Eq. (5.10) can be expressed with the help of symmetrized spherical harmonics (cf. Appendix A and Table IV), the whole computation of the coefficients $C_{l,l'=0}$ can be performed using spherical harmonics. The corresponding formal calculation is described in Appendix B. The actual numerical integrations have been performed using a Monte Carlo technique for the two molecule orientations.

In the first step of the computation of $\overline{V}(\Omega)$, this potential has only an indirect thermal dependence through the value of the lattice parameter $a(T)$:

$$\overline{V}(\Omega) = \overline{V}(\Omega;a) \equiv \overline{V}[\Omega;a(T)]. \quad (5.18)$$

At each temperature, we have thus computed $v_{l,1}^{(1)}$, using the lattice parameter obtained after thermalization and pressure equilibration of our MD computation, the value of which is reported in Table III. The corresponding coefficients for the

TABLE VI. Expansion coefficients $v_0^{(1)}$, $v_4^{(1)}$, $v_6^{(1)}$, and $v_8^{(1)}$ of the orientational mean potential $\overline{V}(\Omega)$ into a basis of symmetrized rotator functions (in kJ/mol).

	135 K	175 K	230 K
$v_0^{(1)}$	−325.1	−365.6	−408.3
$v_4^{(1)}$	7.738	5.943	3.356
$v_6^{(1)}$	9.248	7.360	4.604
$v_8^{(1)}$	2.416	1.994	1.226

three temperatures used in our MD computation are given in Table VI. $\mathscr{P}(\Omega)$, i.e., the various $A_{l,1}^{(1)}$ have then been obtained through Eq. (5.16) again using a Monte Carlo integration technique. The results are given in Fig. 9(a), where we have also given the values already reported in Fig. 4(a) in order to make a precise comparison with the MD simulation results.

C. Discussion

The technique used to compute $v_{l,1}^{(1)}$ and $A_{l,1}^{(1)}$ has been already proposed by Michel *et al.*[8] as the first step towards the prediction of the opdf, but had never been tested up to now. The results are surprisingly good in two respects:

(i) The $A_{l,1}^{(1)}$ are quite similar to the values deduced from the MD simulation, which means that the calculated $\mathscr{P}(\Omega)$ has the same maxima and minima as the computed one.

(ii) The thermal behavior of both opdfs is also remarkably similar.

We shall discuss both aspects in turn.

1. The two-molecule potential energy and $\overline{V}(\Omega)$

It was not *a priori* clear that Eqs. (5.1), (5.9), and (5.13) would lead to a good description of the simulated $\mathscr{P}(\Omega)$. Indeed, if one considers two nearest neighbor molecules in a fcc lattice, one easily convinces oneself that the minimum of their potential energy is realized when both molecules are close to a T_d orientation (i.e., when each of their three $\bar{4}$ molecular symmetry axes coincides with a crystalline fourfold axis), the orientations of the two molecules being different.[41] Indeed, in this situation, the two methyl groups of the two molecules which are in closest contact maximize their relative distance. Nevertheless, a third molecule nearest neighbor to the two first ones is frustrated, because positioning it in any of the two T_d orientations will maximize the methyl group–methyl group interaction for one pair of molecules, while minimizing it for the other. One could not predict whether the partly frustrated opdf suggested by the naive consideration of two molecules only, or the choice of another orientational minimum would be more favorable. It is interesting to find that the simple method of this section leads to a correct prediction of the general shape of $\mathscr{P}(\Omega)$ and to an opdf characterized by D_{2d}, and not T_d orientations.

The present result is important because the method used in this section is known to fail at least in some ODIC phases of ionomolecular crystals, such as NaCN,[42] where the outer atoms of the molecular anion point toward an atomic cation. For pure steric hindrance reasons, such orientations should correspond to the maxima (and not the minima) of the mean orientational potential. We have verified that the shape of the corresponding opdf was not governed by electrostatic interactions between the cation and a distribution of charges on the anion by performing MD simulations of NaCN in which the anionic charge was a monopole located at the center-of-mass of the CN^- ion. Both in our 2D[11] and 3D[43] simulations, the two atoms of the anion still point toward the cations. In other words, the maximum of the opdf $\mathscr{P}^{(\mathrm{MD})}(\Omega)$, obtained in the MD simulation, corresponds to a *maximum* of $\overline{V}(\Omega)$ [and a *minimum* of $\mathscr{P}^{(th)}(\Omega)$] obtained through Eqs. (5.15) and (5.16). The transformation of the minima of $\mathscr{P}^{(th)}(\Omega)$ into maxima can only be obtained if one does not neglect the orientation–translation coupling contribution [the second term of the right-hand side of Eq. (5.7)] and presumably does not perform the decoupling approximations which bring from Eq. (5.2) to Eq. (5.3). It thus seems that the orientation–translation coupling energy is weaker in neopentane than in some of these ionomolecular crystals, a point which is in line with the isotropic character of $d(\mathbf{u})$ analyzed in Sec. IV.

2. Thermal behavior of $\overline{V}(\Omega)$

In order to look more carefully into the thermal behavior of $\mathscr{P}^{(th)}(\Omega)$ obtained through Eqs. (5.15) and (5.16), we have, for each lattice parameter, calculated the corresponding opdf (i.e., the various $A_{l,1}^{(1)}$ coefficients) using the same $v_{l,1}^{(1)}$ for the three different temperatures $T=135$, 175, and 230 K. An example of this calculation is given in Table VII, which compares for each temperature the computed (Sec. III) and the calculated (Sec. V) $A_l^{(1)}$ using for $v_{l,1}^{(1)}$ either the value pertinent to that temperature (second column), or the 135 K value (third column). As can be seen in this table, and in Fig. 9 where the values have been represented graphically, there is not a great difference between both cases; nevertheless, a slightly better overall fit of $\mathscr{P}^{(MD)}(\Omega)$ is obtained with the values of Fig. 9(a). This can be shown by comparing the experimental and the theoretical opdf for 175 and 230 K through the reliability factor

$$\chi=\frac{1}{2}\sum_{i=1}^{2}\frac{\int d\Omega\left|\mathscr{P}^{(th)}(\Omega,T_i)-\mathscr{P}^{(\mathrm{MD})}(\Omega,T_i)\right|^2}{\int d\Omega\left|\mathscr{P}^{(\mathrm{MD})}(\Omega,T_i)\right|^2}, \tag{5.19}$$

where the sum runs over the two temperatures. This reliability factor is $\chi=3.5\times10^{-2}$ for $a(T)=a(T_0)$ and 2.82×10^{-2} for $a(T)$ adjusted at its actual value.

In spite of its obvious weaknesses, the mean potential technique thus gives excellent results at each temperature in the case of neopentane, even at its very first state [Eqs. (5.15), (5.16), and (5.17)]. It is possible that such a good agreement is the result of two compensating effects, namely the neglect of $C_{ll'}$ for $l>8$ and the neglect of the correlation effects. Let us discuss them in turn.

Neglect of $C_{ll'}$ for $l>8$. Even if the potential used in this paper is not as steep as it should be at short distances (cf. the discussion in Sec. IV B), with the values of $|\mathbf{R}_i|$ used in the present calculation, the exp-6 potentials have a quite repulsive character, which is effective for some molecular orienta-

TABLE VII. Expansion coefficients of $\mathscr{P}(\Omega)$. For each temperature, first column: MD simulation; second column: mean-field theory with lattice parameter adjusted for the corresponding temperature; last column: mean-field theory with lattice parameter fixed at its $T = 135$ K value.

	$T = 135$ K			$T = 175$ K			$T = 230$ K		
$A_4^{(1)}$	−0.001	0.009	0.009	−0.016	−0.019	−0.009	−0.030	−0.036	−0.024
$A_6^{(1)}$	−0.292	−0.330	−0.330	−0.234	−0.233	−0.275	−0.159	−0.140	−0.225
$A_8^{(1)}$	0.166	0.154	0.154	0.116	0.065	0.103	0.060	0.011	0.064
$A_{10}^{(1)}$	0.063	0.008	0.008	0.045	0.056	0.069	0.023	0.028	0.054

tions. The truncation in l smoothens the potential and tends to produce too flat an opdf.

Neglect of the correlation effects. Conversely, when one neglects the translation–orientation as well as the orientation–orientation correlations, one allows, in the calculation of $\overline{V}(\Omega)$, for configurations which are avoided in the MD simulation because of their too high energy. This effect increases the stiffness of $\overline{V}(\Omega)$.

In our calculation, these two effects cancel each other more than was anticipated and this cancellation may be partly fortuitous.

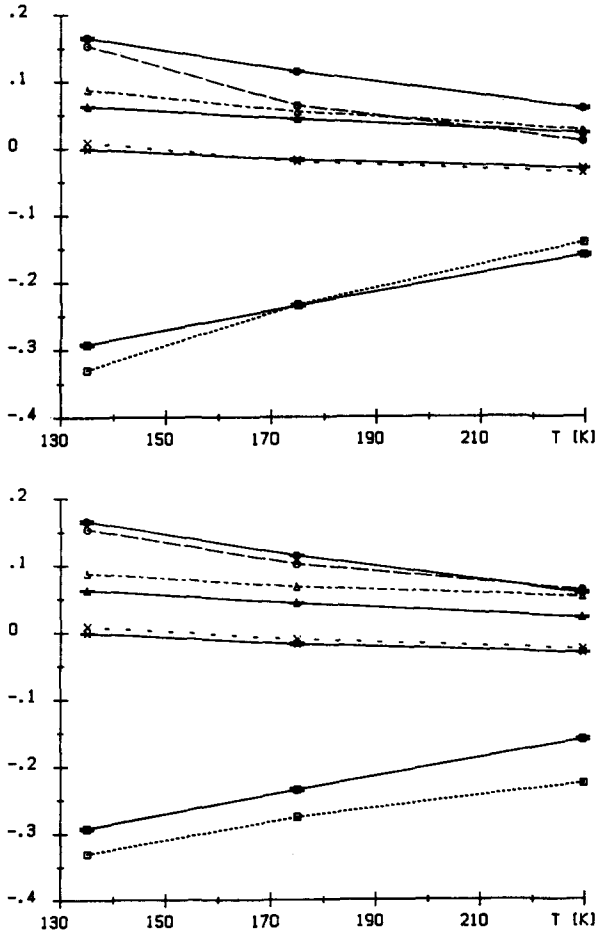

FIG. 9. Variation of the $A_l^{(1)}$ coefficients of the opdf with temperature. Symbols for the coefficients and full lines are the same as in Fig. 4(a). Dotted lines: (a) Mean-field theory with the lattice parameter adjusted for the corresponding tempertaure. (b) Mean-field theory with the lattice parameter fixed at its $T = 135$ K values.

VI. SUMMARY AND FINAL REMARKS

The present MD simulation of the plastic phase of neopentane was undertaken with the double motivation of comparing its results with theoretical predictions as well as with pieces of information extracted from coherent neutron scattering experiments. In the present paper, we have only concentrated ourselves on static properties, i.e., the opdf $\mathscr{P}(\Omega)$ and the dpdf $d(\mathbf{u})$, as well as its second moment the Debye–Waller factor.

Our computation has allowed us to extract and study quantities which had not been obtained in previous comparable works. This is the case, for instance, for the coefficient $A_9^{(2)}$ of the development of the opdf in symmetrized rotator functions; our work represents the first determination of a coefficient of the "second kind" which has been shown not to be zero at least at two of the three considered temperatures. This is also the case for the dpdf. For neopentane, this function turns out to be isotropic and Gaussian with a width much larger than can be produced by the translational phonon contribution alone.

From a theoretical standpoint, at each temperature, $\mathscr{P}(\Omega)$ has been found to be well predicted by a mean potential approach which can be completely determined from the intermolecular potential, once the lattice parameter is known; nevertheless, there is no theory which gives the value of this lattice parameter as a function of temperature, so that in practice, it has to be obtained from a MD or a Monte Carlo computation. Our calculation, which is based *inter alia* on the assumption that one can neglect any correlation between the displacement and the orientation of a given molecule, represents the first reported case in which such a simple theoretical approach properly reproduces the MD simulation results.

Though there exist some weak discrepancies between the present computation and the actual situation in neopentane, presumably related to the too "soft core" character of our intermolecular potential, the simulation fairly describes the real crystal properties. In particular, the general features of the opdf (orientation of its maxima and minima and thermal evolution) are well reproduced. Also, the anomalously large value of the Debye–Waller factor and its peculiar thermal behavior are well-described by our computation, even if our soft core potential leads to too large values for this quantity. We have shown that the isotropic character of the dpdf agrees with the hypothesis of Galam and Depondt[40] that the extra contribution which is responsible for the anomalous thermal behavior of the Debye–Waller factor is the molecular reorientation process.

Let us point out that in all our analyses, we have neglected any correlation between the orientation of a molecule and the displacement of its center-of-mass. Nevertheless, in the vicinity of the plastic-ordered solid phase transition, Galam and Depondt[40] noted that another contribution to the Debye–Waller factor related to this last coupling was presumably necessary to explain the experimental data. As will be shown in the next paper of this series[20] devoted to the study of some dynamical properties, we have found evidence for orientation–translation coupling effects at 135 K when computing some molecular orientation self-correlation functions.

Let us finally remark that the D_{2d} orientation potential well is common to many plastic phases of molecular crystals formed of tetrahedral molecules with the general formula CX_4, such as CH_4,[44] or CBr_4.[45] Such maxima of the opdf have also been obtained in MD simulations performed with rather unrealistic potentials such as that of Dove *et al.*[5] for CBr_4, or Brown and Mountain[27] for neopentane where the methyl group is represented as a single entity.

It is very likely that any intermolecular potential based on atom–atom short-range interactions and a CX_4-like molecule will produce a mean potential $V(\Omega)$ with the same orientational minima. This suggests that in each case the opdf might be rather well-described by a mean-field potential theory, thus, that in each case, the orientation–translation coupling would be weak. It would be interesting to know whether such a prediction is correct and why this orientation–translation effect become more important and makes invalid the mean potential method used here, when long-range forces are included and/or when the shape of the molecule is changed.

ACKNOWLEDGMENTS

The computational time used for the present study has been made available to us by the scientific council of the CCVR. The present paper has also benefitted from long discussions with Ph. Depondt and S. Galam.

APPENDIX A: SYMMETRIC ROTATOR FUNCTIONS FOR A MOLECULE WITH TETRAHEDRAL SYMMETRY

The purpose of this appendix is to derive a practical manner of computing the coefficients $A_l^{(p)}$ of Sec. III, making use not of the rotator functions $\mathscr{R}_l^{\lambda\lambda'}(\Omega)$ (which depend on three variables), but of the more convenient site symmetry adapted surface harmonics $\mathscr{S}_l^{\lambda}(\hat{\mathbf{r}})$ which depend on the two spherical angles only.

Let us suppose that to each molecule we attach a coordinate system in such a way that the C–C bonds point in the [111], [1$\bar{1}\bar{1}$], [$\bar{1}$,1,$\bar{1}$], and [$\bar{1}$,$\bar{1}$,1] directions. Ω, which may be a set of Euler angles, defines the orientation of the molecular axes with respect to the crystal axes. The orthonormality relation between the transformation matrices $M^{\Gamma}_{nn'}(\rho)$ relative to the elements $\rho\in\mathscr{M}$ ($\mathscr{M}$ being the molecular point group) reads:

$$\frac{1}{N}\sum_{k=1}^{N} M^{\Gamma_1}_{n_1n_1'}(\rho_k)M^{\Gamma_2*}_{n_2n_2'}(\rho_k)=\delta_{\Gamma_1\Gamma_2}\delta_{n_1n_2}\delta_{n_1'n_2'}, \tag{A1}$$

where N is the cardinal number of the point group. If we consider the molecular symmetry group being T_d and take for Γ_2 the unity representation A_1, then

$$\frac{1}{N}\sum_{k=1}^{N} M^{\Gamma_1}_{n_1n_1'}(\rho_k)=\delta_{\Gamma_1A_1}. \tag{A2}$$

By definition, for any direction $\hat{\mathbf{r}}_k(\Omega)$ (which is expressed in the crystal axes), one has

$$\mathscr{S}_l^{\lambda}[\hat{\mathbf{r}}_k(\Omega)]=\sum_{\lambda'}\mathscr{R}_l^{\lambda\lambda'}(\Omega)\mathscr{M}_l^{\lambda'}(\hat{\mathbf{r}}_k), \tag{A3}$$

where $\hat{\mathbf{r}}_k$ is the same direction expressed in the molecular coordinate system. Furthermore, if in this coordinate system $\hat{\mathbf{r}}_k$ is deduced from a direction $\hat{\mathbf{r}}_0$ by the rotation $\rho_k\in\mathscr{M}$, then by definition of the symmetry adapted surface harmonics

$$\mathscr{M}_l^{\lambda'}(\hat{\mathbf{r}}_k)=\sum_{n''}M^{\Gamma'}_{n'n''}(\rho_k)\mathscr{M}_l^{\lambda''}(\hat{\mathbf{r}}_0) \tag{A4}$$

where λ' and λ'' differ only by their last index (n' or n'').

With the help of Eqs. (A3) and (A4), we can write

$$\begin{aligned}\frac{1}{N}\sum_{k=1}^{N}\mathscr{S}_l^{\lambda}[\hat{\mathbf{r}}_k(\Omega)]&=\frac{1}{N}\sum_{\lambda'}\mathscr{R}_l^{\lambda\lambda'}(\Omega)\sum_{k=1}^{N}\mathscr{M}_l^{\lambda'}(\hat{\mathbf{r}}_k)\\&=\frac{1}{N}\sum_{\Gamma',\mu',n'}\mathscr{R}_l^{\lambda\lambda'}(\Omega)\sum_{n''}\left[\sum_{k=1}^{N}M^{\Gamma'}_{n'n''}(\rho_k)\right]\mathscr{M}_l^{\lambda''}(\hat{\mathbf{r}}_0),\end{aligned} \tag{A5}$$

where, by definition, the $\hat{\mathbf{r}}_k$ have been obtained from the same $\hat{\mathbf{r}}_0$ by application of all the elements $\rho_k\in\mathscr{M}$. By reason of Eq. (A2), we can replace the summation over k:

$$\begin{aligned}\frac{1}{N}\sum_{k=1}^{N}\mathscr{S}_l^{\lambda}[\hat{\mathbf{r}}_k(\Omega)]&=\sum_{\Gamma',\mu',n'}\mathscr{R}_l^{\lambda\lambda'}(\Omega)\delta_{\Gamma'A_1}\mathscr{M}_l^{\lambda'}(\hat{\mathbf{r}}_0)\\&=\sum_{\mu'}\mathscr{R}_l^{\lambda A_1}(\Omega)\mathscr{M}_l^{A_1}(\hat{\mathbf{r}}_0).\end{aligned} \tag{A6}$$

If for a given l, the representation A_1 is included only once in the corresponding l subspace, we can suppress the sum over μ'. Furthermore, if we chose $\hat{\mathbf{r}}_0$ to be the direction of one of the four C–C bonds, only a sum over four vectors has to be performed, since for all rotations $\rho_k\in T_d$, a C–C bond is always mapped onto another C–C bond. Thus, we finally have

$$\mathscr{R}_l^{\lambda A_1}(\Omega)=\frac{1}{4}\frac{\sum_{k=1}^{4}\mathscr{S}_l^{\lambda}[\hat{\mathbf{r}}_k(\Omega)]}{\mathscr{M}_l^{A_1}(\hat{\mathbf{r}}_0)}, \tag{A7}$$

where $\hat{\mathbf{r}}_k(\Omega)$ are the four unit vectors pointing in the direction of the C–C bonds described in the crystal axes, $\mathscr{M}_l^{A_1}$ is the surface harmonics with full molecular symmetry, and $\hat{\mathbf{r}}_0$ is a unit vector pointing in the direction of an arbitrary C–C bond described in the molecular axes.

The same formalism can be used to find a relation between the $\mathscr{R}_l^{\lambda A_2}$ and the $\mathscr{S}_l^{\lambda}$ (when one wants to calculate the coefficients of the second kind). Indeed, as A_2 is a one-dimensional representation, the character $\chi_{A_2}(\rho_k)$ is its transformation matrix. Multiplying both sides of Eq. (A5) by the character $\chi_{A_2}(\rho_k)$, one can therefore write

$$\frac{1}{N}\sum_{k=1}^{N}\mathscr{S}_l^{\lambda}[\hat{\mathbf{r}}_k(\Omega)]\chi_{A_2}(\rho_k) = \frac{1}{N}\sum_{\Gamma',\mu',n'}\mathscr{R}_l^{\lambda\lambda'}(\Omega) \times\sum_{n''}\left[\sum_{k=1}^{N}M_{n'n''}^{\Gamma'}(\rho_k)\chi_{A_2}(\rho_k)\right]\mathscr{M}_l^{\lambda''}(\hat{\mathbf{r}}_0). \quad \text{(A8)}$$

Using Eq. (A1) with $\Gamma' = A_2$, we can again suppress the summation over k, so that for l subspaces which only once contain the A_2 representation, we finally arrive at an equation analogous to Eq. (A7), namely

$$\mathscr{R}_l^{\lambda A_2}(\Omega) = \frac{1}{24}\frac{\sum_{k=1}^{24}\chi_{A_2}(\rho_k)\mathscr{S}_l^{\lambda}[\hat{\mathbf{r}}_k(\Omega)]}{\mathscr{M}_l^{A_2}(\hat{\mathbf{r}}_0)}, \quad \text{(A9)}$$

where, in this case, $\hat{\mathbf{r}}_0$ [and hence the corresponding $\hat{\mathbf{r}}_k(\Omega)$] must not be any symmetry direction in order to assure that the denominator will not vanish.

APPENDIX B: EVALUATION OF THE ORIENTATIONAL ONE PARTICLE POTENTIAL

The one particle potential can be developed in a series of symmetric rotator functions (5.9):

$$\overline{V}(\Omega) = \sum_l[(v_l^{(1)}\mathscr{R}_l^{(1)}(\Omega) + v_l^{(2)}\mathscr{R}_l^{(2)}(\Omega)], \quad \text{(B1)}$$

where up to $l = 10$, the only first kind coefficients arise for $l = 0, 4, 6, 8$, and 10. Using Eq. (A7), we can thus calculate these coefficients by

$$v_l^{(1)} = \frac{1}{4\cdot\mathscr{M}_l^{A_1}(\hat{\mathbf{r}}_0)}\sum_{k=1}^{4}\int d\Omega\,\overline{V}(\Omega)\mathscr{S}_l^{A_{1g}}[\hat{\mathbf{r}}_k(\Omega)], \quad \text{(B2)}$$

where the $\hat{\mathbf{r}}_k(\Omega)$ are expressed in the crystal axes. It is easier to perform the numerical calculation in some coordinate system (X_1,Y_1,Z_1), where the Z_1 axis coincides with the vector joining the centers-of-mass of two molecules. For this purpose, we concentrate first on the interaction potential between the central molecule and the molecule located in the [110] direction ($Z_1 \| [110]$) and choose Y_1 to be alined with the crystal z axis. We then expand the $\mathscr{S}_l^{A_{1g}}(\hat{\mathbf{r}})$ in a series of cubic harmonics $\mathscr{S}_l(\hat{\mathbf{R}}_1)$ written in the (X_1,Y_1,Z_1) axes. This is best accomplished in two steps: First, we perform the transformation to axes which are defined through the relations

$$X_1 \to Y, \quad Y_1 \to Z, \quad Z_1 \to X, \quad \text{(B3)}$$

which gives

$$\mathscr{S}_l^{\lambda'}(\hat{\mathbf{R}}) = \sum_{\lambda}\beta_l^{\lambda'\lambda}\mathscr{S}_l^{\lambda}(\hat{\mathbf{R}}_1). \quad \text{(B4)}$$

Then, we write

$$X \to \frac{1}{\sqrt{2}}(x+y), \quad Y \to \frac{1}{\sqrt{2}}(-x+y), \quad Z \to z, \quad \text{(B5)}$$

and therefore

$$\mathscr{S}_l^{A_{1g}}(\hat{\mathbf{r}}) = \sum_{\lambda'}\gamma_l^{A_{1g}\lambda'}\mathscr{S}_l^{\lambda'}(\hat{\mathbf{R}}). \quad \text{(B6)}$$

Now, we write the functions $\mathscr{S}_l^{\lambda}(\hat{\mathbf{R}}_1)$ as a linear combination of the $Y_l^m(\hat{\mathbf{R}}_1)$, because the interaction potential has $C_{\infty v}$ symmetry around the Z_1 axis. Using Eqs. (B2), (B4), and (B6), we can finally write for the coefficients

$$v_l^{(1)} = \frac{1}{16\pi^2\cdot\mathscr{M}_l^{A_1}(\hat{\mathbf{r}}_0)}\sum_{\lambda'}\sum_{\lambda}\gamma_l^{A_{1g}\lambda'}\beta_l^{\lambda'\lambda}\alpha_l^{\lambda m} \times\sum_{k=1}^{4}\int d\Omega\,d\Omega_1\,V(\Omega,\Omega_1)\,Y_l^m[\hat{\mathbf{R}}_1^{(k)}(\Omega)]. \quad \text{(B7)}$$

The integrals appearing in Eq. (B7) were calculated numerically by Monte Carlo integration. The advantage of this method is that due to the $C_{\infty v}$ symmetry mentioned above non-zero integrals exist only for $m = 0$. Due to this last remark, it turns out to be more convenient to work backwards and to write

$$Y_l^0(\hat{\mathbf{R}}_1) = \sum_{\lambda}(\alpha^{-1})_l^{0\lambda}\mathscr{S}_l^{\lambda}(\hat{\mathbf{R}}_1), \quad \text{(B8)}$$

$$\mathscr{S}_l^{\lambda}(\hat{\mathbf{R}}_1) = \sum_{\lambda'}(\beta^{-1})_l^{\lambda\lambda'}\mathscr{S}_l^{\lambda'}(\hat{\mathbf{R}}), \quad \text{(B9)}$$

$$\mathscr{S}_l^{\lambda'}(\hat{\mathbf{R}}) = \sum_{\lambda_1}(\gamma^{-1})_l^{\lambda'\lambda_1}\mathscr{S}_l^{\lambda_1}(\hat{\mathbf{r}}), \quad \text{(B10)}$$

where in Eq. (B10), we are only interested in the $\lambda_1 = A_{1g}$ terms, as all the others will vanish when one will take into account the 11 other nearest neighbors.

The $(\alpha^{-1})_l^{0\lambda}$ coefficients are given, for all values of l, in the Altman-Cracknell tables[34] in numerical values. They are reproduced under algebraic form in Table VIII, where one finds that for even l, λ spans only the A_{1g} or the E_g^1 representations (where the index 1 labels that component of E_g which is symmetric in X_1 and Y_1). Furthermore,

$$(\beta^{-1})_l^{A_{1g}\lambda} = \delta_{\lambda,A_{1g}},$$

and

$$(\beta^{-1})_l^{E_g^1\lambda} = -\frac{1}{2}\delta_{\lambda,E_g^1} + \frac{\sqrt{3}}{2}\delta_{\lambda,E_g^2}.$$

Finally, $(\gamma^{-1})_l^{E_g^2A_{1g}}$ is equal to zero for symmetry reasons, but the $(\gamma^{-1})_l^{\lambda'A_{1g}}$ must be computed algebraically for each l, for $\lambda' = A_{1g}$ and $\lambda' = E_g^1$, separately. This yields

$$Y_4^0(\hat{\mathbf{R}}^{(1)}) = -\frac{1}{8}\sqrt{\frac{7}{3}}\mathscr{S}_4^{A_{1g}}(\hat{\mathbf{r}}) + \cdots,$$

$$Y_6^0(\hat{\mathbf{R}}^{(1)}) = \frac{13}{8\sqrt{8}}\mathscr{S}_6^{A_{1g}}(\hat{\mathbf{r}}) + \cdots,$$

TABLE VIII. Coefficients $(\alpha^{-1})_l^{0\lambda}$ for $l = 4$, 6, and 8. Note that for $l = 8$, there are two E_g representations, but Y_8^0 projects only on one of them.

l	A_{1g}	E_g^1
4	$\frac{1}{2}\sqrt{\frac{7}{3}}$	$\frac{1}{2}\sqrt{\frac{5}{3}}$
6	$\frac{\sqrt{2}}{4}$	$\frac{\sqrt{14}}{4}$
8	$\frac{\sqrt{33}}{8}$	$\frac{\sqrt{31}}{8}$

$$Y_8^0(\hat{\mathbf{R}}^{(1)}) = \frac{\sqrt{11}}{64}\left(\frac{17}{\sqrt{3}} - \frac{7\sqrt{11}}{2\sqrt{31}}\right)\mathscr{S}_8^{A_{1g}}(\hat{\mathbf{r}}) + \cdots$$

$$\simeq 0.4006 \cdot \mathscr{S}_8^{A_{1g}}(\hat{\mathbf{r}}) + \cdots \qquad \text{(B11)}$$

where $\cdots$ stands for all the representations with $\lambda_1 \neq A_{1g}$.

[1] *The Plastically Crystalline State*, edited by J. N. Sherwood (Wiley, New York, 1979) and references therein.

[2] D. G., Bounds, M. L. Klein, and I. R. McDonald, Phys. Rev. Lett. **46**, 1682 (1981); M. L. Klein, Y. Ozaki, and I. R. McDonald, J. Phys. C **15**, 4993 (1982).

[3] M. L. Klein, I. R. McDonald, and Y. Ozaki, J. Chem. Phys. **79**, 5579 (1983).

[4] G. S. Pawley and G. W. Thomas, Phys. Rev. Lett. **48**, 410 (1982); G. S. Pawley, A. M. Brass, M. T. Dove, and K. J. Refson, J. Chim. Phys. **82**, 249 (1985).

[5] M. Dove, J. Phys. C **19**, 3325 (1986); M. Dove and R. M. Lynden-Bell, *ibid.* **19**, 3343 (1986).

[6] R. Fourret (private communication).

[7] R. M. Lynden-Bell, I. R. McDonald, and M. L. Klein, Mol. Phys. **48**, 1093 (1983).

[8] K. H. Michel and J. Naudts, J. Chem. Phys. **65**, 977 (1977).

[9] K. H. Michel and K. Parlinski, Phys. Rev. B **31**, 1823 (1985).

[10] D. Sahu and S. D. Mahanty, Phys. Rev. B **26**, 2981 (1982).

[11] M. Yvinec, Mol. Cryst. Liq. Cryst. **89**, 359 (1982).

[12] M. Yvinec, Mol. Cryst. Liq. Cryst. **109**, 303 (1984).

[13] Ph. Buchet and R. M. Pick, Europhys. Lett. **2**, 709 (1987); J. Phys. **48**, 821 (1987).

[14] D. E. Williams, J. Chem. Phys. **47**, 4680 (1967).

[15] M. Meyer and G. Ciccotto, Mol. Phys. **56**, 1235 (1985).

[16] M. Meyer, C. Marhic, and G. Ciccotto, Mol. Phys. **58**, 723 (1986); G. Ciccotti, M. Ferrario, E. Memeo, and M. Meyer, Phys. Rev. Lett. **59**, 2574 (1987).

[17] O. Hardouin-Duparc, in Disorder in Molecular Solids, organized by H. Szwarc, Garchy, France, 5–7 July 1989.

[18] B. Denise, Ph. Depondt, M. Debeau, and P. Schweiss, J. Phys. (Paris) **48**, 615 (1987).

[19] Ph. Depondt and M. Debeau, J. Phys. (Paris) **48**, 1513 (1987).

[20] W. Breymann and R. M. Pick (to be published).

[21] W. Breymann and R. M. Pick, Europhys. Lett. **8**, 429 (1989).

[22] W. Breymann and R. M. Pick, Europhys. Lett. **6**, 227 (1988).

[23] W. Breymann, Ph. Depondt, and R. M. Pick, Can. J. Chem. **66**, 798 (1988).

[24] R. V. Gopala and J. N. Joarder, J. Phys. C **14**, 4745 (1981).

[25] L. S. Bartell and W. F. Bradford, J. Mol. Struct. **37**, 113 (1977).

[26] This contrasts with the calculation of Brown and Mountain Ref. 27 who concentrated themselves more on the properties of the liquid phase than on those of the plastic phase, and described the methyl group as a single entity.

[27] R. D. Mountain and A. C Brown, J. Chem. Phys. **82**, 4236 (1985).

[28] In order to take into account the thermal expansion, the lattice parameter was readjusted for each temperature at the beginning of the run, keeping the mean pressure in a reasonable range between 11 and 18 MPa.

[29] W. Press, Acta. Crystallogr. A **29**, 257 (1973); W. Press and A. Hüller, *ibid.* **29**, 252 (1973).

[30] M. Yvinec and R. M. Pick, J. Phys. (Paris) **41**, 1045 (1980).

[31] M. Yvinec and R. M. Pick, J. Phys. (Paris) **41**, 1053 (1980).

[32] A. Hüller and J. W. Kane, J. Chem. Phys. **61**, 3599 (1974).

[33] C. von der Lage and H. A. Bethe, Phys. Rev. **71**, 612 (1947).

[34] C. J. Bradley and A. P. Cracknell, *The Mathematical Theory of Symmetry in Solids* (Clarendon, Oxford, 1972), p. 51ff.

[35] $p(\hat{\mathbf{r}})$ can be expanded into a series of site symmetry adapted surface harmonics (i.e., cubic harmonics in the present case): $p(\hat{\mathbf{r}}) = \Sigma_{l\lambda}\, a_l^\lambda \mathscr{S}_l^\lambda(\hat{\mathbf{r}})$. For a given l, there is a one-to-one correspondence between the coefficients a_l^λ and $A_l^{\lambda A_1}$, if the unity representation is contained only once in the l subspace. This fact explains why we can here discuss the effect of series truncation on $p(\hat{\mathbf{r}})$ rather than on $\mathscr{P}(\Omega)$. Nevertheless, if an l subspace contains, e.g., twice the unity representation of the molecular point group, the coefficients a_l^λ will be a linear combination of the two coefficients $A_l^{\lambda A_1(1)}$ and $A_l^{\lambda A_1(2)}$. As this is the case for the T_d group for $l \geqslant 12$, $p(\hat{\mathbf{r}})$ would not be an unambiguous representation of $\mathscr{P}(\Omega)$, if terms with $l \geqslant 12$ had been included in Eq. (3.4).

[36] Another truncation effect could be the occurrence of artificial secondary extrema in $p(\hat{\mathbf{r}})$. This effect, which has been reported by Denise *et al.* Ref. 18, does not appear in our case.

[37] R. G. Della-Valle, P. F. Fracassi, R. Righini, and S. Califano, J. Chem. Phys. **74**, 179 (1983).

[38] R. Righini, S. Califano, and S. N. Walmsley, J. Chem. Phys. **50**, 113 (1980).

[39] R. Righini, K. Maki, and M. L. Klein, Chem. Phys. Lett. **80**, 301 (1981).

[40] S. Galam and Ph. Depondt, Europhys. Lett. **5**, 43 (1988).

[41] There are only two such possible T_d orientations.

[42] J. M. Rowe, D. G. Hinks, D. L. Price, S. Susman, and J. J. Rush, J. Chem. Phys. **58**, 2039 (1973).

[43] M. H Ambard, thesis, Paris (1987) (unpublished).

[44] W. Press and A. Hüller, Phys. Rev. Lett. **30**, 1207 (1972).

[45] M. More, J. Lefebvre, and R. Fourret, Acta Crystallogr. B **33**, 3862 (1977); G. Dolling, B. M. Powell, and V. F. Sears, Mol. Phys. **37**, 1859 (1979).